Int. J. Solids Structures Vol. 27, No. 8, pp. 1035–1046, 1991
Printed in Great Britain.

0020–7683/91 $3.00 + .00

THE EFFECT OF RESTRAINING FORCE ON SPRINGBACK

C.-C. CHU
Room S2046, Scientific Research Laboratories, Ford Motor Company, P.O. Box 2053, Dearborn, MI 48121-2503, U.S.A.

(*Received* 28 *December* 1989)

Abstract—In this paper, the effects of restraining force on springback are analyzed by following the stress–strain development across the sheet thickness for flanged channels, stretch-bent under plane-strain conditions. An isotropic–kinematic hardening rule is assumed for the material, so that the elastic–plastic unloading behavior involved in forming procedures with complicated loading paths can be more accurately simulated. Good agreement is found between analytical and experimental results on simple springback, side-wall curls and their respective dependence on the in-plane restraining force. Furthermore, the significance of individual parameters on general springback phenomena is clearly identified.

INTRODUCTION

Springback is generally defined as the additional deformation of a structural component, resulting from the removal of forming loads. Such a deformation may contribute towards significant deviation from a desired shape, and thus cause quality concerns. Since the springback problem has generally been observed to worsen with increased material tensile strength (Davies, 1984), it becomes very important to be able to predict springback quantitatively as well as qualitatively in the auto industry's pursuit of higher strength materials for weight reduction. While there have been quite a few experiments characterizing the importance of various parameters on springback (for example Davies, 1984; Liu, 1988; Hayashi, 1984), there has only been limited success in establishing simple theoretical models widely applicable to practical springback problems. Specifically, all analytical attempts (for example Duncan and Bird, 1978; Thompson and Ellen, 1985; Wang, 1984; Wenner, 1983) were only for simple bending cases and assumed an elastic unloading behavior. This paper features (1) the adoption of an isotropic–kinematic hardening rule, which more accurately stimulates the material behavior during complex loading; (2) the effectiveness of in-plane restraining force on reducing springback; and (3) the importance of individual parameters in affecting springback.

PROBLEM FORMULATION AND RESULTS

The two problems studied here are generally known as simple springback and side-wall curl. Both are featured in Fig. 1, where the cross-section of a wide piece of sheet metal being formed into a flanged channel by the downward movement of a punch into the die cavity is sketched. A typical sheet section at the bottom of the channel, which is bent to the punch radius during forming, relaxes its unbalanced internal stresses by altering its shape after the forming load is removed. This is referred to as simple springback. On the other hand, elements along the side wall are drawn in from the flange area and go through a more complicated bending–straightening path. The removal of the forming loads then results in a curled instead of a straight wall.

The problems are simplified by assuming that both the bottom portion and the side-wall portion of the channel are uniformly formed. Therefore, modeling the in-plane stress (σ) and strain (ε) developments across the sheet thickness (denoted hereafter as 0 to t in the z-direction) *in a representative section* from each of the above-mentioned two areas, is sufficient to predict springback. It is further assumed that plane-strain conditions prevail and that the plane section remains plane during bending; that is, if the neutral axis position

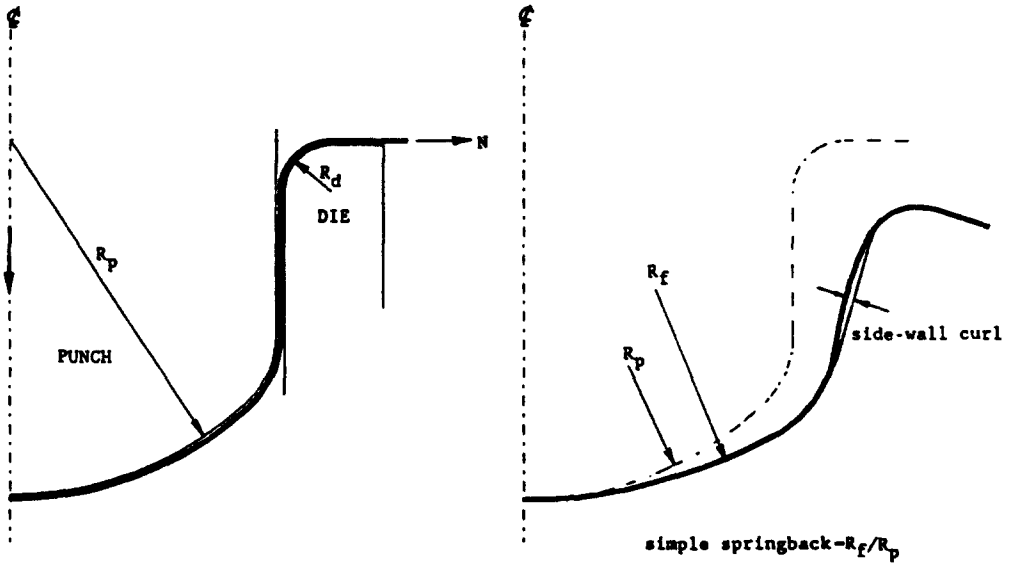

Fig. 1. A sketch of the stretch-draw forming of a flanged channel and the springback phenomena.

(z_n) and the radius of curvature (κ) for the deformed section are known, the in-plane strain distribution through sheet thickness is approximately written as

$$\varepsilon(z) = \kappa(z - z_n).$$

Here, a power-law type of in-plane stress–strain curve is adopted:

$$|\sigma|/\sigma_y = \begin{cases} |\varepsilon|/\varepsilon_y & \text{for } |\varepsilon| < \varepsilon_y \\ (|\varepsilon|/\varepsilon_y)^n & \text{for } |\varepsilon| > \varepsilon_y \end{cases}. \tag{1}$$

Note that the absolute value is used so that eqn (1) applies to both tensile and compressive loading conditions. As will be explained in the Appendix, the above normalized stress–strain curve is derived from a conventional equivalent stress–equivalent strain curve. The in-plane yield stress and yield strain, denoted by σ_y and ε_y, respectively, in eqn (1), are accordingly defined in terms of uniaxial properties of the material. The constants for several steels investigated in this paper are listed at the end of the Appendix.

An isotropic–kinematic hardening rule is employed here to describe the behavior of the material during reversed loading. This hardening rule is more accurate than the isotropic hardening rule in predicting elastic–plastic reverse loading behavior, and is easier to formulate (Chu, 1987). For the essentially one-dimensional problem at hand, the model reduces to the following simple stress–strain relationship for a reverse loading path initiated from a plastic state (σ_r, ε_r):

$$|\Delta\sigma|/(2\sigma_y) = \begin{cases} |\Delta\varepsilon|/2\varepsilon_y & \text{for } |\Delta\varepsilon| < 2\varepsilon_y \\ (|\Delta\varepsilon|/(2\varepsilon_y))^n & |\Delta\varepsilon| > 2\varepsilon_y; \end{cases} \tag{2}$$

where $|\Delta(\ )|$ denotes the absolute value of the progression of a quantity from $(\ )_r$, where reverse loading is initiated. Figure 2 illustrates the initial in-plane stress–strain curve, denoted by (0), for monotonic loading from a virginal state, followed consecutively by three reverse loading paths which are likely to occur in the present study. According to the adopted hardening model, the reverse loading path proceeds by eqn (2) (a two-fold magnification of the initial stress–strain curve) until the most recently established flow stress level is reached, at which point it coincides with and then resumes the previously interrupted path. For

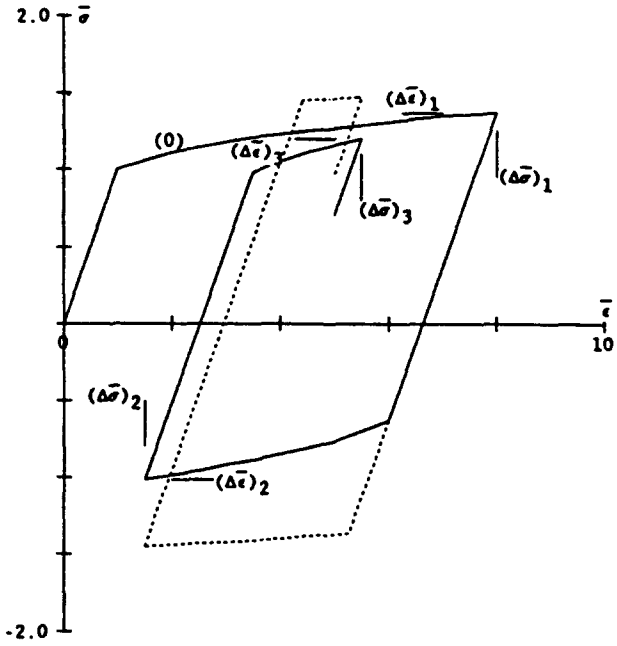

Fig. 2. The in-plane stress–strain behavior for a complex loading pattern: the solid curves for the isotropic–kinematic hardening model and the dotted curves for the isotropic hardening model.

comparison purposes, the stress–strain behavior based on the classical isotropic hardening model, shown by the dotted lines, is also included.

The in-plane stretching force (N) and the bending moment about the mid-surface (M) can now be obtained in terms of κ and z_n, by integrating the stress function $\sigma[\varepsilon(z)]$ in the z-direction:

$$N = \int_0^t \sigma[\kappa(z-z_n)]\,\mathrm{d}z, \quad M = \int_0^t \sigma[\kappa(z-z_n)]\cdot(z-t/2)\,\mathrm{d}z.$$

Henceforward, normalized quantities ($\bar{}$) are used not only to simplify the equations, but also to clearly identify the importance of individual parameters; that is, length is normalized by sheet thickness (t), stress and strain are normalized by their corresponding in-plane yield values ε_y and σ_y, curvature is normalized by (ε_y/t), and (N, M) is normalized by $(\sigma_y t, \sigma_y t^2/6)$. The above equations are therefore rewritten as

$$\bar{N} = \int_0^1 \bar{\sigma}[\bar{\kappa}(\bar{z}-\bar{z}_n)]\,\mathrm{d}\bar{z}, \quad \bar{M} = 6\int_0^1 \bar{\sigma}[\bar{\kappa}(\bar{z}-\bar{z}_n)]\cdot(\bar{z}-\tfrac{1}{2})\,\mathrm{d}\bar{z}.$$

Simple springback

The process that leads to the simple springback phenomenon can be described by the following series of proportional paths: (1) The sheet is formed from a stress-free state to $(\bar{\kappa}_0, \bar{N}_0)$, where $\bar{\kappa}_0 = t/[\varepsilon_y(R_p+z_n)]$ with R_p denoting the punch radius, and $\bar{N}_0$ the given normalized in-plane force. (2) The sheet is uniformly released of the restraining force, from $(\bar{\kappa}_0, \bar{N}_0)$ to $(\bar{\kappa}_0, \bar{N}=0)$. (3) After the punch is removed, the sheet reaches a state which is free from external forces $(\bar{N}=0, \bar{M}=0)$. Note that the above unloading paths (2) and (3) more closely follow the actual forming process than the more commonly used proportional path, which unloads directly from $(\bar{\kappa}_0, \bar{N}_0)$ to $(\bar{N}=0, \bar{M}=0)$.

An example of the strain and stress distribution across the thickness at the end of each proportional path is sketched in Fig. 3, where dotted curves from the previous path are included to show the stress and strain progression. The corresponding equations which

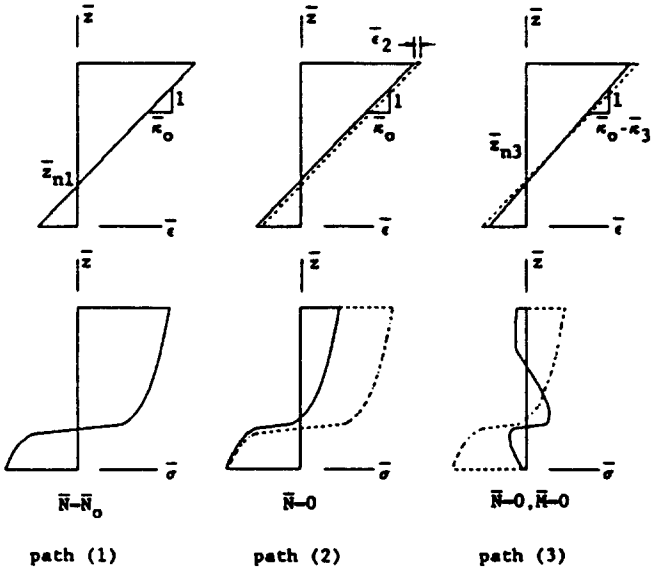

Fig. 3. An example of the stress and strain development across the sheet thickness for a simple springback problem.

satisfy the prescribed conditions are:

For path (1),

$$\bar{N}_1(\bar{z}_{n1}) = \bar{N}_0 = \int_0^{\bar{z}_{n1}-1/\bar{\kappa}_0} -[-\bar{\kappa}_0(\bar{z}-\bar{z}_{n1})]^n \,d\bar{z} + \int_{\bar{z}_{n1}-1/\bar{\kappa}_0}^{\bar{z}_{n1}+1/\bar{\kappa}_0} \bar{\kappa}_0(\bar{z}-\bar{z}_{n1})\,d\bar{z} + \int_{\bar{z}_{n1}+1/\bar{\kappa}_0}^{1} [\bar{\kappa}_0(\bar{z}-\bar{z}_{n1})]^n \,d\bar{z}. \quad (3\text{-}1)$$

For path (2),

$$\bar{N}_2(\bar{\varepsilon}_2) = 0 = \int_0^{\bar{z}_{n1}-(1-\bar{\varepsilon}_2)/\bar{\kappa}_0} -[\bar{\varepsilon}_2 - \bar{\kappa}_0(\bar{z}-\bar{z}_{n1})]^n \,d\bar{z} + \int_{\bar{z}_{n1}-(1-\bar{\varepsilon}_2)/\bar{\kappa}_0}^{\bar{z}_{n1}+1/\bar{\kappa}_0} [\bar{\kappa}_0(\bar{z}-\bar{z}_{n1}) - \bar{\varepsilon}_2]\,d\bar{z} + \int_{\bar{z}_{n1}+1/\bar{\kappa}_0}^{1} [(\bar{\kappa}_0(\bar{z}-\bar{z}_{n1}))^n - \bar{\varepsilon}_2]\,d\bar{z}. \quad (3\text{-}2)$$

For path (3),

$$\bar{N}_3(\bar{z}_{n3}, \bar{\kappa}_3) = 0 = -\int_0^{\bar{z}_{n3}+(2-\bar{\varepsilon}_2)/\bar{\kappa}_3} \bar{\kappa}_3(\bar{z}-\bar{z}_{n3})\,d\bar{z} - \int_{\bar{z}_{n3}+(2-\bar{\varepsilon}_2)/\bar{\kappa}_3}^{1} [2((\bar{\varepsilon}_2 + \bar{\kappa}_3(\bar{z}-\bar{z}_{n3}))/2)^n - \bar{\varepsilon}_2]\,dz,$$

$$\bar{M}_3(\bar{z}_{n3}, \bar{\kappa}_3) = 0 = \bar{M}_2 - \int_0^{\bar{z}_{n3}+(2-\bar{\varepsilon}_2)/\bar{\kappa}_3} 6\bar{\kappa}_3(\bar{z}-\bar{z}_{n3})\,\bar{z}\,d\bar{z} - \int_{\bar{z}_{n3}+(2-\bar{\varepsilon}_2)/\bar{\kappa}_3}^{1} 6[2((\bar{\varepsilon}_2 + \bar{\kappa}_3(\bar{z}-\bar{z}_{n3}))/2)^n - \bar{\varepsilon}_2]\,\bar{z}\,d\bar{z}, \quad (3\text{-}3)$$

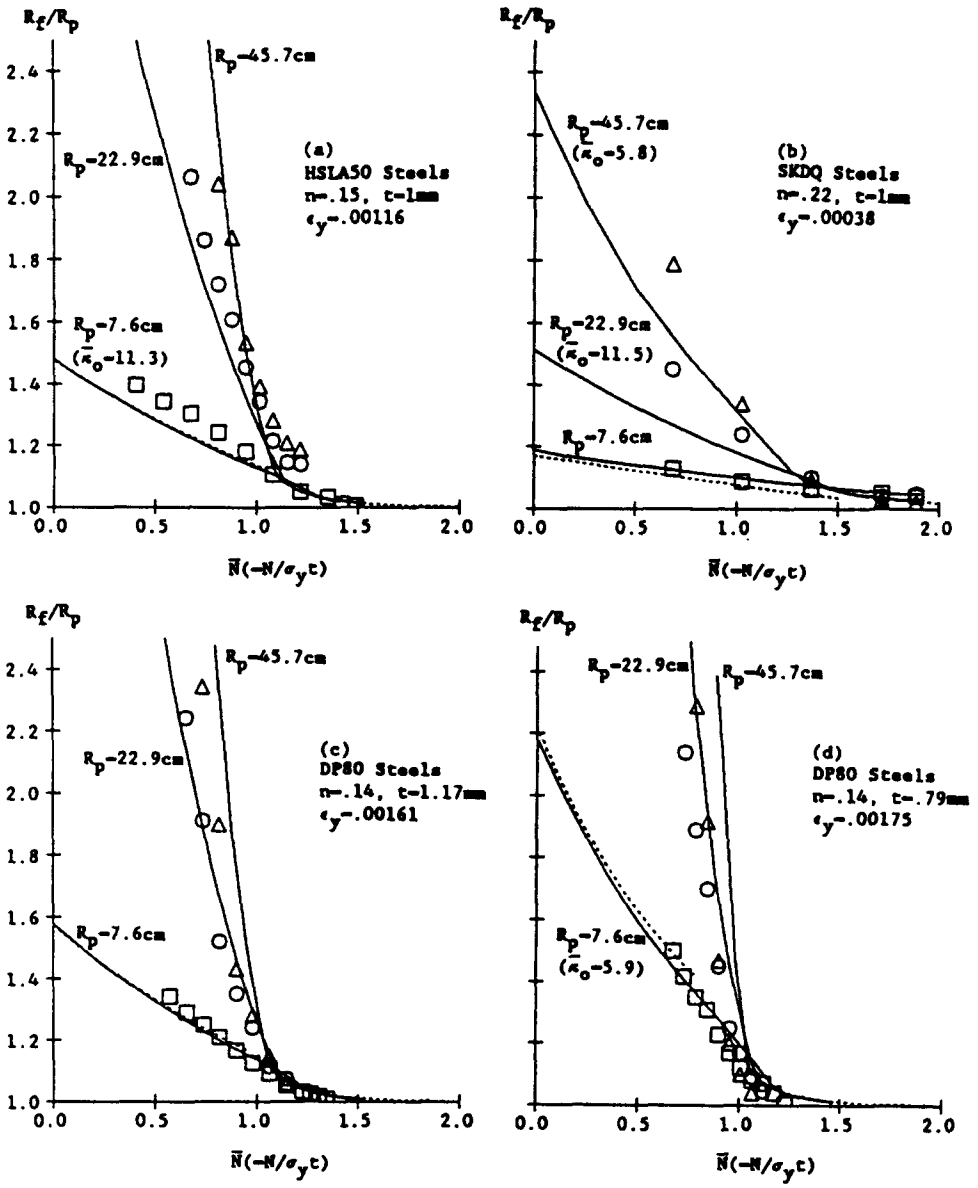

Fig. 4. Analytical and experimental simple springback results as a function of normalized in-plane restraining force for various materials.

Here, the numerical subscripts indicate the path with which the quantities are associated. Note that eqns (3) only apply if $\bar{\varepsilon}_{n1} > 1/\bar{\kappa}_0$, $\bar{\varepsilon}_2 < 2$ and $\bar{\varepsilon}_2 + \bar{\kappa}_3(1-\bar{z}_{n3}) > 2$. When these conditions change as a result of neutral axis movement, eqns (3) need to be correctly modified so that the integration limits remain in the range (0, 1) and the complicated material behavior along different loading branches is taken into account. The above-mentioned non-linearity of the equations about $\bar{z}_{n1}$, $\bar{\varepsilon}_2$, $\bar{z}_{n3}$ and $\bar{\kappa}_3$ requires solution by a computer program which was written to handle the trial and error scheme used here.

The final normalized curvature $\bar{\kappa}_f$ is $(\bar{\kappa}_0 - \bar{\kappa}_3)$. The simple springback, which is defined as the ratio of the final radius of curvature to the designed one, is then obtained by

$$R_f/R_p = \bar{\kappa}_0/\bar{\kappa}_f.$$

The calculated simple springback results, which are affected by the in-plane stretching force, are displayed as solid curves in Figs 4 for several steels. The following major analytical conclusions are worth noting:

(a) The problem parameters ε_y, R_p and $1/t$ all have the same effect on springback since they only enter the equilibrium equations, such as eqns (3), via the same dimensionless curvature measure $\bar{\kappa}_0$, which was defined earlier as $(t/R_p\varepsilon_y)$. Therefore, the observed increase in both simple springback and the slope of the $(R_f/R_p)-\bar{N}_0$ curve, as a result of higher R_p values for individual materials, can also be seen for materials with larger yield strain values.

(b) A decrease in the strain hardening exponent n, which is the only other dimensionless parameter that enters the equilibrium equations, moves the $(R_f/R_p)-\bar{N}_0$ curve slightly to the left while still maintaining its general shape. This can be seen by comparing the curves in Figs 4 with similar $\bar{\kappa}_0$ values, which are shown in Figs 4 for this purpose.

(c) An in-plane restraining force of the order of $(\sigma_y t)$, or approximately a unit of normalized force as shown in Figs 4, can remove most of the simple springback. In fact, this limiting value of N_0 which is required for effective springback reduction is shown later to simply mean a force large enough to stretch-bend the complete sheet, plastically.

The above findings are substantiated by very good agreement, both qualitatively and quantitatively, between the predicted curves and experimental data (from Liu, 1988) which are represented by open symbols in Figs 4.

It is shown in the following that for two special cases, further useful results for simple springback can be obtained in closed-form without resorting to tedious calculations. The first case involves a small in-plane stretching force and relatively severe bending, where $\bar{\kappa}_0 \gg 1$ can be assumed. Both eqns (3-1) and (3-2) apply here and are approximately solved by a series expansion about $\bar{z}_{n1} = \frac{1}{2}$. That is, by replacing $\bar{z}_{n1}$ with $(\frac{1}{2}-\delta)$ in the equations and neglecting higher order terms of δ, we obtain

$$\begin{aligned}\bar{z}_{n1} &\simeq \tfrac{1}{2}[1-\bar{N}_0/\alpha]\\ \bar{\varepsilon}_2 &\simeq 2\bar{\kappa}_0\bar{N}_0/[(\alpha\bar{\kappa}_0+2)+\bar{N}_0(\bar{\kappa}_0/\alpha-2n)]\\ \bar{M}_2 &\simeq 3(\beta-\gamma\bar{N}_0);\end{aligned}$$

where $\alpha = (\frac{1}{2}\bar{\kappa}_0)^n$, $\beta = \alpha/(n+2)$ and $\gamma = [(\frac{1}{2}\bar{\kappa}_0)-2\alpha n/(n+1)]/[2\alpha+\bar{\kappa}_0]$. If the unbending path (3) is an elastic process, we then have $(\bar{z}_{n3}, \bar{\kappa}_3) = (\frac{1}{2}, 2\bar{M}_2)$. The simple springback is therefore,

$$R_f/R_p = \bar{\kappa}_0/(\bar{\kappa}_0-2\bar{M}_2) \simeq [(1-6\beta/\bar{\kappa}_0)+\bar{N}_0(6\gamma/\bar{\kappa}_0)]^{-1}. \tag{4}$$

The range of $\bar{N}_0$ values necessary for this prediction to be appropriate can be extended at the most to $\bar{N}_1(\bar{z}_{n1} = 1/\bar{\kappa}_0)$, which is approximately $\bar{\kappa}_0^n/(n+1)$.

The second closed-form approximation is obtained for $\bar{N}_0$ values larger than $\bar{N}_1(\bar{z}_{n1} = -1/\bar{\kappa}_0)$; that is, when the complete plate is plastically stretch-bent. By assuming $(-\bar{z}_{n1}) \gg 1$, it can be shown that

$$\bar{N}_0 \simeq (-\bar{\kappa}_0\bar{z}_{n1})^n, \quad \text{and} \quad \bar{M}_2 \simeq \tfrac{1}{2}n(-\bar{\kappa}_0\bar{z}_{n1})^{n-1}.$$

The simple springback therefore approaches a limiting value,

$$(R_f/R_p)_{lim} = \bar{\kappa}_0/(\bar{\kappa}_0-2\bar{M}_2) = [1-n(\bar{N}_0)^{(n-1)/n}]^{-1}. \tag{5}$$

The limiting value is seen to be independent of the degree of bending, $\bar{\kappa}_0$. This is in agreement with experimental results for different R_p values (and hence different $\bar{\kappa}_0$ values), which merge with each other at large $\bar{N}$ in Figs 4.

Approximations according to eqns (4) and (5) for the most severely bent case where $R_p = 7.62$ mm, are shown in Figs 4 as dotted curves. They appear to be very accurate in obtaining (a) the effectiveness of $\bar{N}_0$ in reducing springback and (b) the limiting value of springback. Both features are important in determining the restraining force and the punch radius required to form a desired curvature.

Side-wall curl

For a typical section in the side-wall area, the process occurring is composed of a slightly more complicated history: (1) It is formed from ($\bar{N}=0$, $\bar{M}=0$) to ($\bar{\kappa}_0, \bar{N}_0$). (2) The sheet is then straightened to ($\bar{\kappa}_w, \bar{N}_0$), where the degree of straightening depends on the geometric constraints such as the die gap. (3) The clamping force is removed but $\bar{\kappa}_w$ remains geometrically constrained in the die cavity. That is, the condition ($\bar{\kappa}_w, \bar{N}_0=0$) has to be satisfied. (4) An external force-free state ($\bar{M}=0$, $\bar{N}=0$) is reached.

The side-wall curl has been experimentally measured by the depth of the crown formed between a chord, of a carefully chosen length, and the curled wall (Davies, 1984). It should be noted that such a measurement of a single value is appropriate only when the resulting side wall has a uniform radius of curvature; that is, when $\bar{\kappa}_w$ in paths (2) and (3) maintains a constant value for all sections along the wall. This is approximately the case in the experimental studies of side-wall curl by Davies (1984), but not so in the more realistic channel forming set-up by Liu (1988). While the former provides a simplified procedure to shed light on the importance of individual parameters on curl, the latter, in emphasizing the effects of the in-plane force on preventing curl, shows the complexity involved in a more realistic drawing process.

We first analyze the experiments of Davies (1984), for which it is noted that $\bar{N}_0=0$, $\bar{\kappa}_w=0$ and $\bar{\kappa}_0 \simeq t/[\varepsilon_y R_d]$, where R_d is the die radius. For this comparatively simple problem involving complex loading, both the current isotropic–kinematic hardening model and the classical isotropic hardening model are used to show the differences in predicting springback by the two models. By assuming that $\bar{\kappa}_0 \gg 1$, the residual moment at the end of path (3) can be easily obtained:

$$(\bar{M}_3)_{\text{two kin}} = 12\left\{\int_0^{1/\bar{\kappa}_0}(\bar{\kappa}_0\bar{z})\bar{z}\,d\bar{z}+\int_{1/\bar{\kappa}_0}^{1/2}(\bar{\kappa}_0\bar{z})^n\bar{z}\,d\bar{z}-\int_0^{2/\bar{\kappa}_0}(\bar{\kappa}_0\bar{z})\bar{z}\,d\bar{z}-\int_{2/\bar{\kappa}_0}^{1,2}2^{1-n}(\bar{\kappa}_0\bar{z})^n\bar{z}\,d\bar{z}\right\}$$

$$\simeq 3(1-2^{1-n})(\tfrac{1}{2}\bar{\kappa}_0)^n/(n+2),$$

$$(\bar{M}_3)_{\text{iso}} = 12\left\{\int_{1/\bar{\kappa}_0}^{2^{1-n}/\bar{\kappa}_0}[(\bar{\kappa}_0\bar{z})^n-(\bar{\kappa}_0\bar{z})]\bar{z}\,d\bar{z}-\int_{2^{1-n}/\bar{\kappa}_0}^{1/2}[2(\bar{\kappa}_0\bar{z}-(\bar{\kappa}_0\bar{z})^n)]^n\bar{z}\,d\bar{z}\right\}$$

$$\simeq -3\bar{\kappa}_0^n/(n+2).$$

The side-wall curl is then calculated by

$$\begin{aligned}(\text{curl}) &= R_f-\sqrt{[R_f^2-(l/2)^2]} \simeq l^2/(8R_f), \quad (\text{assuming } (l/2R_f)^2 \ll 1)\\ &= \tfrac{1}{8}l^2\cdot\kappa_f/2 = -\tfrac{1}{4}l^2\bar{M}_3\varepsilon_y/t\\ &= f(n)\cdot\tfrac{1}{4}l^2(\varepsilon_y)^{1-n}(R_d)^{-n}(t)^{n-1},\end{aligned} \tag{6}$$

where l denotes the afore-mentioned chord length, $R_f(=1/\kappa_f=t/(\bar{\kappa}_f\varepsilon_y))$ is the final radius of curvature and $f(n)$ is $[3(2^{1-2n}-2^{-n})/(n+2)]$ for the isotropic–kinematic hardening model, and is $[3/(n+2)]$ for the isotropic hardening model. Examples of the predicted dependence of curl on sheet thickness t, without the in-plane restraining force, are shown in Figs 5. The solid curves from the isotropic–kinematic hardening model are thus $(2^{1-2n}-2^{-n})$ times more conservative than the dotted curves from the isotropic hardening model. The experimental data, represented by filled symbols, are seen to be in good qualitative agreement with analytical results; but quantitatively they seem to scatter between the curves predicted by the two models.

In the following, the effects of post-straining on curl, as tested in Davies (1984), will be studied. The sheet here is strained from the straightened state $\bar{\varepsilon}(\bar{z})\equiv 0$ to $\bar{\varepsilon}(\bar{z})\equiv\bar{\varepsilon}_p$. By assuming that $\bar{\varepsilon}_p \ll \bar{\kappa}_0$, the residual moments after post-straining are:

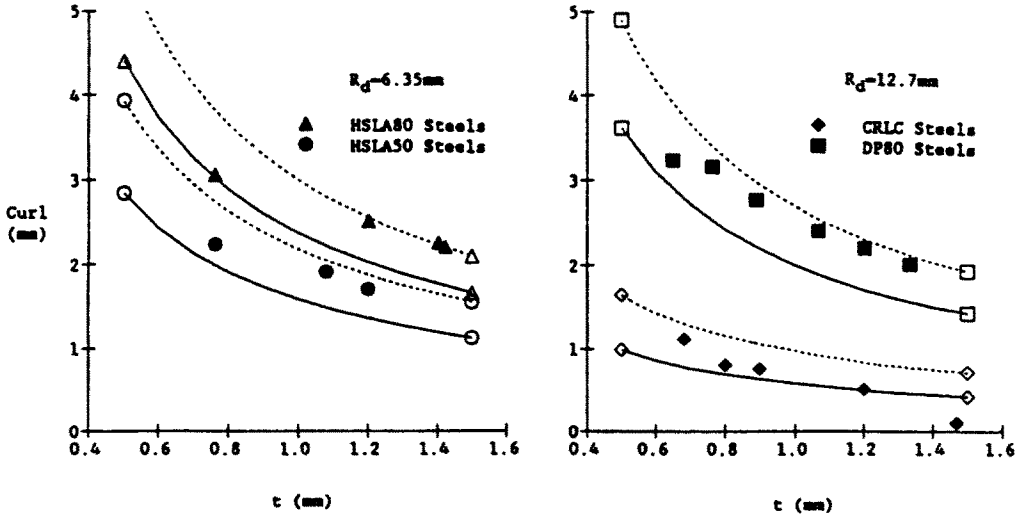

Fig. 5. Analytical and experimental side-wall curl results as a function of sheet thickness for four different steels: the solid curves are for the isotropic–kinematic hardening model and the dotted curves are for the isotropic hardening model.

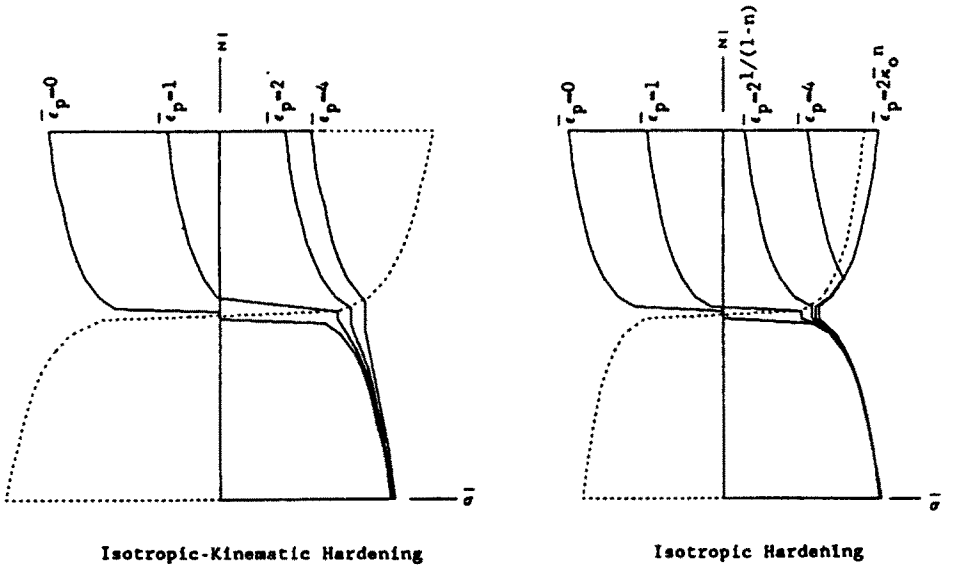

Fig. 6. The stress development in the simple curl problem following bending (the dotted curve), straightening (the $\bar{\varepsilon}_p = 0$ curve) and a progressive amount of post-straining.

$$(\bar{M}_r)_{\text{iso-kin}} \simeq \begin{cases} \bar{M}_3 + \frac{3}{4}\bar{\varepsilon}_p & \text{for } \bar{\varepsilon}_p \leqslant 2 \\ \bar{M}_3 + 3/2 \cdot (\frac{1}{2}\bar{\varepsilon}_p)^n & \text{for } \bar{\varepsilon}_p > 2 \\ \bar{M}_3 + \frac{3}{4}\bar{\varepsilon}_p & \text{for } \bar{\varepsilon}_p \leqslant 2^{1/(1-n)}, \end{cases} \tag{7}$$

$$(\bar{M}_r)_{\text{iso}} \simeq \begin{cases} \bar{M}_3 + \frac{3}{4}\bar{\varepsilon}_p - 3n/(n+2) \cdot \frac{1}{4}^{(1+n)/n} \cdot \bar{\varepsilon}_p^{(n+2)/n}/\bar{\kappa}_0^2 & \text{for } 2^{1/(1-n)} < \bar{\varepsilon}_p < 2\bar{\kappa}^n{}_0 \\ 0 & \text{for } \bar{\varepsilon}_p \geqslant 2\bar{\kappa}_0^n. \end{cases}$$

These are obtained by following the stress developments for various amounts of post-straining, as illustrated in Figs 6 for both hardening rules. The amount of curl is thus

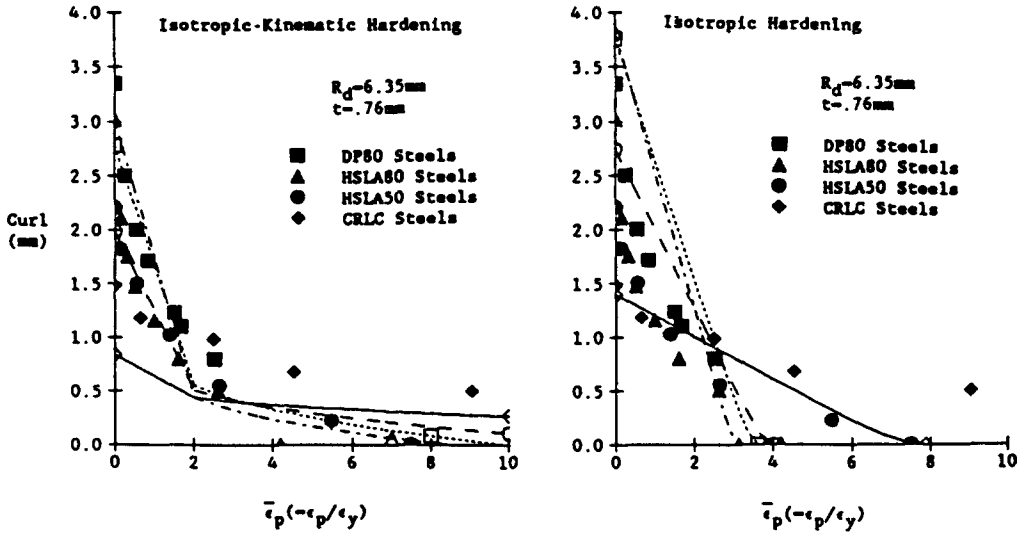

Fig. 7. Analytical and experimental results for side-wall curl as a function of the amount of normalized post-straining.

calculated by (curl) $= -\frac{1}{4}l^2\bar{M}_t\varepsilon_y/t$ and displayed in Figs 7. The comparison between experimental data, represented by filled symbols, and analytical curves, marked at the ends with corresponding symbols, shows that the currently adopted isotropic–kinematic hardening model predicts the effectiveness of post-straining on curl reduction more accurately than the isotropic hardening model (except for mild steels where the analytical curve seems to lie consistently below the experimental data by a significant amount). We therefore emphasize the important finding discovered from the isotropic–kinematic hardening model here: a unit increase of normalized post-straining up to two, or an increase of post-straining by ε_y up to $2\varepsilon_y$, can effectively reduce curl by $(\frac{3}{4}\cdot\frac{1}{4}l^2/t)$. This significance of post-straining by $2\varepsilon_y$, which is equivalent to post-stretching by a force $(\sigma_y t)$, in largely eliminating curl was not readily observed in the study by Davies (1984).

As mentioned earlier, in most of the realistic drawing operations, geometric conditions are too complex to warrant a closed-form analysis such as the one presented above. The following attempts to predict the effect of in-plane restraining force on the curl for the channel forming operation with a larger-than-thickness die gap (Liu, 1988), which serves as an example to illustrate the difficulties involved. As sketched in Fig. 8, if the in-plane stretching force is not large enough to completely straighten the sheet from its curved shape (permitted by a finite die gap) to $\bar{\kappa}_w = 0$ during forming, the side wall, while remaining in the die cavity, then assumes a relatively complex form. That is, the sections that are drawn to different depths are subjected to varying degrees of unbending: from $\bar{\kappa}_w = 0$ near the bottom to some finite $\bar{\kappa}_w$ value near the entrance of the die cavity. The resulting wall is therefore of constantly changing curvature, which means that the single-valued experimental curl measurement does not fully represent the deviation of a curled wall from a desirable straight shape. Furthermore, the present analysis carried out on section level cannot be expected to predict such a curl well. Nevertheless, it is assumed here that the deformed wall can be approximately represented by an arc with an average radius of curvature, so that a single-valued curl can be obtained and compared with experimental results. This average radius of curvature is arbitrarily assumed here to vary proportionately with the in-plane restraining force as follows: when $\bar{N}_0 = 0$, $\bar{\kappa}_w$ is determined by geometric constraints as noted in Fig. 8. (This deformed curvature is obtained by simulating the wall in the die cavity with a constrained cantilever beam.) As $\bar{N}_0$ increases, $\bar{\kappa}_w$ decreases linearly to $\bar{\kappa}_w = 0$ at $\bar{N}_0 = \bar{N}_1(\bar{z}_{n1} = 0)$.

A computer program is again used to carry out the trial-and-error method and the side-wall curls are presented in Figs 9 as functions of the in-plane stretching forces. The

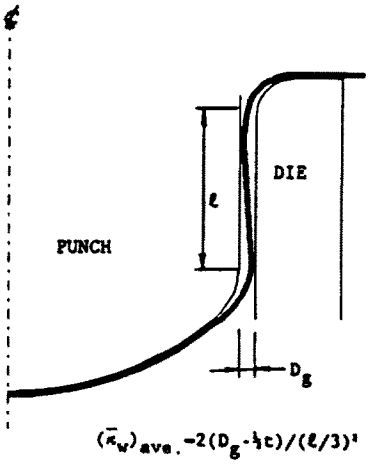

Fig. 8. A sketch of the shape complexity in a realistic stretch-draw forming with the die gap larger than the sheet thickness.

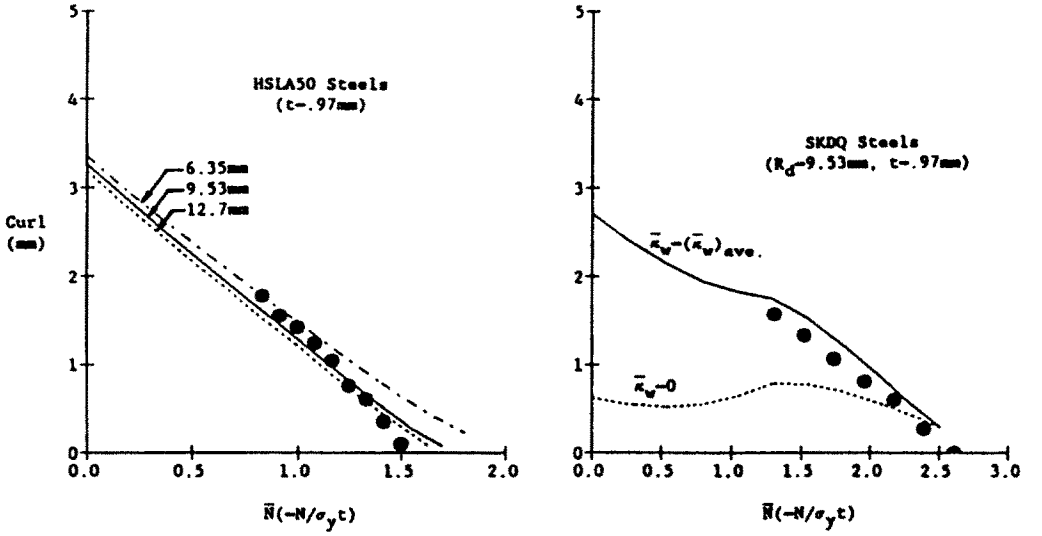

Fig. 9. Analytical and experimental results for curl as a function of normalized in-plane restraining force for two steels.

experimental curl data, shown in Liu (1988) against the in-plane force measured in the horizontal flange section instead of in the vertical side-wall section, are shifted to the right by a factor of $e^{\mu\pi/2}$ to indicate the effect of Coulomb friction over the die radius, with μ arbitrarily assumed to be 0.1, and are represented by filled symbols in Figs 9. The observed agreement between experimental and analytical results is surprisingly good. Also displayed in Fig. 9a are the results as predicted for two other R_d values. Both the predicted minor dependence of curl on die radius and the slight decrease of slope with increasing R_d are in qualitative agreement with experimental results in Liu (1988) (excluding the R_d = 18 mm case where recoiling may have occurred (Hayashi, 1984)). In Fig. 9b the dotted curve, obtained by setting $\bar{\kappa}_w \equiv 0$, is for a drawing operation with die gap equal to sheet thickness. The significant difference between the solid and dotted curves therefore represents the

influence of die gap on curl. The slope change, or the change of effectiveness of $\bar{N}_0$ on reducing curl, observed in Fig. 9b near $\bar{N}_0 = 1$, is noted to be caused by plastic, instead of elastic, reverse loading behavior in the final unbending path.

CONCLUSIONS

This study has succeeded in analytically predicting springback and its dependence on in-plane restraining force. The important conclusions are:

(1) Springback is found to mainly depend on two dimensionless parameters: the strain hardening exponent of the material n and the degree of bending, defined by $t/(R\varepsilon_y)$.

(2) An in-plane restraining force of the order of the yield strength can eliminate most of the simple springback and simple curl. However, in a more realistic drawing operation than studied here, curl is found to be even more sensitive to parameters such as die gap, which affects the amount of straightening preceded curling.

(3) The isotropic–kinematic hardening model adopted here is found not only to simplify the formulation, but also predict springback phenomena more accurately than the classical isotropic hardening, in particular, for materials with higher yield strength.

(4) Complications caused by geometric parameters such as die gap, which are not included in the equilibrium equations, may be satisfactorily accounted for by modifying the prescribed loading conditions.

REFERENCES

Chu, C.-C. (1987). The analysis of multiaxial cyclic problems with an anisotropic hardening model. *Int. J. Solids Structures* **21**(5), 569–579.

Davies, R. G. (1984). "Side-wall curl" in high-strength steels. *J. Appl. Metalworking* **3**(2), 120–126.

Duncan, J. L. and Bird, J. E. (1978). Approximate calculations for draw die forming and their application to aluminum alloy sheet. *Proc. 10th Biennial Congress IDDRG*, Warwick, England, pp. 45–52.

Hayashi, Y. (1984). Analysis of surface defects and side wall curl in press forming. *Proc. 13th Biennial Congress IDDRG*, Melbourne, Australia, pp. 565–580.

Liu, Y. C. (1988). The effect of restraining force on shape deviations in flanged channels. *J. Engng Mater. Tech., ASME Trans.* **110**(4), 389–394.

Thompson, N. E. and Ellen, C. H. (1985). A simple theory for "side-wall curl". *J. Appl. Metalworking* **4**(1), 39–42.

Wang, N. M. (1984). Efficiency in sheet metal forming. *Proc. 13th Biennial Congress IDDRG*, Melbourne, Australia, pp. 133–147.

Wenner, M. L. (1983). On work hardening and springback in plane strain draw forming. *J. Appl. Metalworking* **2**(4), 277–287.

APPENDIX

The adopted power-law type of equivalent stress-equivalent strain curve is

$$\tau_e = \begin{cases} E\varepsilon_e & \text{for } \varepsilon_e \leqslant (\varepsilon_e)_y \\ K\varepsilon_e^n & \varepsilon_e > (\varepsilon_e)_y. \end{cases}$$

where E denotes Young's modulus and n and K are material constants determined from uniaxial tensile data. In order to have a continuous σ_e–ε_e curve, the yield strain is obtained by $E(\varepsilon_e)_y = K(\varepsilon_e)_y^n$. That is, $(\varepsilon_e)_y = (K/E)^{1/(1-n)}$ and therefore, $(\sigma_e)_y = E(\varepsilon_e)_y$. Note that the calculated $(\sigma_e)_y$ is different from the measured yield stress. For the plane-strain problem considered here, the major in-plane stress and strain, denoted by σ and ε respectively, are related to their equivalent counterpart by $\sigma = c\sigma_e$ and $c\varepsilon = \varepsilon_e$, with $c = (1+r)/\sqrt{(1+2r)}$ where r is the anisotropy parameter of the material. The in-plane stress strain relationship therefore can be derived as follows:

$$\sigma = \begin{cases} c^2 E\varepsilon & \text{for } \varepsilon \leqslant \varepsilon_y (= (\varepsilon_e)_y/c) \\ c^{1+n} K\varepsilon^n & \varepsilon > \varepsilon_y. \end{cases}$$

By normalizing the above equation against the in-plane yield stress $\sigma_y (= c(\sigma_e)_y = c^2 E\varepsilon_y = c^{1+n} K\varepsilon_y^n)$, we obtain

$$\sigma/\sigma_y = \begin{cases} \varepsilon/\varepsilon_y & \text{for } \varepsilon \leqslant \varepsilon_y \\ (\varepsilon/\varepsilon_y)^n & \varepsilon > \varepsilon_y. \end{cases}$$

The materials constants for several steels studied here are listed below.

For simple springback studies:

	n	K (MPa)	r	
HSLA50 steels	0.15	745	0.96	E = 206, 850 MPa for all steels
DP80 steels (t = 1.17 mm)	0.14	931	1.01	
DP80 steels (t = 0.79 mm)	0.14	1000	1.01	
SKDQ steels	0.22	559	2.02	

For curl studies:

	n	K (MPa)	r
CRLC steels	0.23	487	1.5
HSLA50 steels	0.15	745	0.96
HSLA80 steels	0.11	942	1.0
DP80 steels	0.14	1000	1.01
SKDQ steels	0.2	503	1.88